VII International Conference on Computational Methods for Coupled Problems in Science and Engineering
COUPLED PROBLEMS 2017
M. Papadrakakis, E. Oñate and B. Schrefler (Eds)

MODELLING PIEZOELECTRIC ENERGY HARVESTERS BY A FINITE INTEGRATION TECHNIQUE FORMULATION FOR ELECTROMECHANICAL COUPLED PROBLEMS

F. MORO[*], D. DESIDERI[*], A. DORIA[*], A. MASCHIO[*], C. MEDÉ[*], AND L. CODECASA[†]

[*] Dipartimento di Ingegneria Industriale
Università di Padova
Via Gradenigo 6/A, 35131 Padova, Italy
e-mail: federico.moro@unipd.it

[†] Dipartimento di Elettronica, Informazione e Bioingegneria
Politecnico di Milano
Via Ponzio 34/5, 20133 Milano.Italy

Key words: Coupled Problems, Multiphysics, Piezoelectric, Energy Harvesting, Finite Integration Technique, Cell Method.

Abstract. A detailed analysis and optimization of piezoelectric devices, which nowadays are of widespread use in electronic applications, requires numerical analysis. Numerical models based on the Finite Element Method (FEM) have already been proposed in literature. The Finite Integration Technique (FIT) provides stable and consistent discretization schemes for coupled multiphysics problems. A FIT formulation with unstructured meshes, for 2-D/3-D coupled electromechanical static or dynamic problems, is presented. Piezoelectric bimorph cantilevers, with a realistic multilayered geometry, can be analyzed. Comparisons with FEM show the validity and the accuracy of the method.

1 INTRODUCTION

Piezoelectric materials are nowadays of widespread use for producing actuators, sensors, and energy harvesters for feeding ultra-low power electronics [1]. Analytical models are well-assessed and important tools for designing and optimizing piezoelectric devices [2]. Lumped circuit models are derived for instance in control applications [3]. Non ideal conditions like clamping setup, local variations in geometry and material properties, and residual stress may significantly affect the device performance, and in particular its resonance frequency. Accurate numerical electromechanical 3-D coupled models are thus required. The FEM analysis of piezoelectric structures is thoroughly documented in the literature [4]. In particular, thin-plate finite elements were proposed to limit the amount of problem unknowns [5].

The Finite Integration Technique or, equivalently, the Cell Method (CM) are numerical techniques, which provide field equations directly in algebraic form, thus suitable for computer

coding [6,7]. These are alternative to FEM because the field problem is formulated in a circuit-like manner in terms of degrees of freedom (DoFs), i.e. volume and surface integrals of vector fields and scalar potentials. This feature is suitable for modelling multiphysics problems, where different types of couplings occur. A coupling between different physics is provided in [8] by solving an electro-thermal problem with CM. In [9] different computational domains, which can be discretized independently, are matched by a CM formulation. An example of coupling between different numerical methods, e.g. the CM and the Boundary Element Method (BEM), is finally provided in [10]. The extension of FIT and CM to elastic problems has been more complex due to mathematical structure of elasticity, inherently different from electromagnetic problems. A first attempt of CM elastic formulation was proposed by Tonti in [11]. The role of topological operators in elasticity was evidenced in [12]. Finally, CM formulations for multiphysics problems including elasticity were proposed in [6,7,13].

The basic idea here is to extend this algebraic approach for analysing piezoelectric coupled problems, where the elastic problem is coupled to the electrostatic problem via constitutive relationships.

2 FIT PIEZOELECTRIC FORMULATION

Let $\Omega \in \mathbb{R}^d$ $(d = 2, 3)$ be a piezoelectric body with boundary $\Gamma = \partial\Omega$. The response to external body-surface forces is ruled by dynamic equilibrium and compatibility equations, which exhibit a more simple representation when the small displacement assumption holds true. This condition is well verified in typical piezo-mechanical applications like energy harvesters, actuators, and sensors. Similarly, electrostatics is governed by curl-free constraint and charge conservation. These equations are complemented by local piezoelectric relationships:

$$\mathrm{T_{ij}} = \mathrm{c^{E}_{ijkh}}\,\mathrm{S^{kh}} - \mathrm{e_{kij}}\mathrm{E^{k}}, \tag{1}$$

$$\mathrm{D_{i}} = \mathrm{e_{ikh}}\mathrm{S^{kh}} + \varepsilon^{\mathrm{S}}_{\mathrm{ik}}\mathrm{E^{k}}, \tag{2}$$

where $\mathrm{T_{ij}}$, $\mathrm{S^{kh}}$ are the stress and the strain tensors, $\mathrm{D_i}$, $\mathrm{E^k}$ are the electric displacement and electric fields, and $\mathrm{c^{E}_{ijkh}}$, $\mathrm{e_{ikh}}$, $\varepsilon^{\mathrm{S}}_{\mathrm{ik}}$ are the elastic, piezoelectric, and dielectric tensors. In (1) and (2) the Einstein summation convention is implicitly assumed.

In FIT formulations problem variables are DoFs defined on geometric entities like points, lines, surfaces, and volumes. The computational domain is first meshed into tetrahedrons so that a primal grid $\mathcal{G}_\Omega$ with N nodes and E edges is built. Dual grids $\tilde{\mathcal{G}}_\Omega$ and $\tilde{\mathcal{G}}_\Gamma$ are defined on Ω and Γ by taking the barycentric subdivisions of primal grids $\mathcal{G}_\Omega$ and $\mathcal{G}_\Gamma$ (the restriction of $\mathcal{G}_\Omega$ to Γ). The *augmented dual grid* is built by joining volume and boundary grids as $\tilde{\mathcal{G}}_{\Omega\Gamma} = \tilde{\mathcal{G}}_\Omega \cup \tilde{\mathcal{G}}_\Gamma$ [14]. The following incidence matrices are defined for discretization on dual grids: $\mathbf{G}_\Omega$ (edges to nodes on $\mathcal{G}_\Omega$), $\widetilde{\mathbf{D}}_\Omega = -\mathbf{G}_\Omega^{\mathrm{T}}$ (volumes to faces on $\tilde{\mathcal{G}}_\Omega$), $\widetilde{\mathbf{D}}_{\Omega\Gamma}$ (volumes on $\tilde{\mathcal{G}}$ to faces on on $\tilde{\mathcal{G}}_\Gamma$).

For the mechanical problem the following arrays of DoFs are defined for any i–th spatial component (with $i = 1 \ldots d$): displacements on primal nodes n, $\mathbf{s}^i = (s^i_n)$; line integrals of the displacement gradient $x^{kh} = s^{k,h}$ along primal edges e, $\mathbf{x}^i = (x^i_e)$, where $x^i_e = \int_e \mathrm{x^{ij}t_j}\, d\gamma$ and $\mathrm{t_j}$ is unit tangent vector along e; fluxes of the stress tensor on dual faces $\tilde{f}$, $\tilde{\mathbf{t}}_i = (\tilde{t}_{i\tilde{f}})$, where

$\tilde{t}_{i\tilde{f}} = \int_{\tilde{f}} \mathrm{T}_{ij}\, \mathrm{n}^{\mathrm{j}}\, d\sigma$ and n^{j} unit normal vector to face $\tilde{f}$. For the electrostatic problem, arrays of DoFs are: electric potentials at primal nodes $\mathbf{\Phi} = (\varphi_n)$; electric voltages along primal edges, $\mathbf{u} = (u_e)$, where $u_e = \int_e \mathrm{E}^j\, \mathrm{t}_{\mathrm{j}}\, d\gamma$ is the line integral of the electric field E^j; fluxes of electric displacement D_j on dual faces $\tilde{\mathbf{d}} = (\tilde{d}_{\tilde{f}})$, where $\tilde{d}_{\tilde{f}} = \int_{\tilde{f}} \mathrm{D}_j\, \mathrm{n}^{\mathrm{j}}\, d\sigma$.

3.1 Static coupled problem

In a FIT scheme, similar to a circuit-like electric problem formulation, topological and constitutive relationships have to be constructed in order to fully constrain arrays of DoFs. Topological relations on the primal grid for the mechanical and electrical variables are:

$$\mathbf{x}^i = \mathbf{G}_\Omega\, \mathbf{s}^i, \tag{3}$$

$$\mathbf{e} = -\mathbf{G}_\Omega\, \mathbf{\Phi}, \tag{4}$$

The topological relationships for the dual grid are the equilibrium equations for electrostatics and mechanics:

$$\widetilde{\mathbf{D}}_\Omega\, \tilde{\mathbf{t}}_i + \widetilde{\mathbf{D}}_{\Omega\Gamma}\, \tilde{\mathbf{t}}_{\Gamma,i} = \tilde{\mathbf{f}}_i, \tag{5}$$

$$\widetilde{\mathbf{D}}_\Omega\, \tilde{\mathbf{d}} + \widetilde{\mathbf{D}}_{\Omega\Gamma}\, \tilde{\mathbf{d}}_\Gamma = \tilde{\mathbf{q}}, \tag{6}$$

where $\tilde{\mathbf{t}}_{\Gamma,i}$, $\tilde{\mathbf{d}}_\Gamma$ are stress tensor and dielectric displacement fluxes on the boundary dual faces, $\tilde{\mathbf{f}}_i = (\tilde{f}_i)$ is the array of external body forces.

By integrating on dual faces strain tensor and electric displacement in (1) and (2), the following discrete relationships are obtained:

$$\tilde{\mathbf{t}}_i = \mathbf{C}_{ij}\, \mathbf{x}^j - \mathbf{E}_i\, \mathbf{e}, \tag{7}$$

$$\tilde{\mathbf{d}} = \mathbf{E}_j^{\mathrm{T}} \mathbf{x}^j + \boldsymbol{\varepsilon}\, \mathbf{e}, \tag{8}$$

where $\mathbf{C}_{ij} = (c_{ij,ee\prime})$, $\mathbf{E}_i = (E_{i,ee\prime})$, $\boldsymbol{\varepsilon} = (\varepsilon_{ee\prime})$ are respectively the elastic, piezoelectric, dielectric constitutive matrices, all of size $E \times E$. These matrices are assembled from local matrices constructed as described in [6].

For instance, the elastic matrix is obtained as follows. For a given tetrahedron τ, edge vectors and dual face vectors (within the tetrahedron), depicted in Fig. 1, are computed for any primal edge. By assuming an affine displacement distribution within any tetrahedron τ, the displacement gradient is uniform within τ. For any edge $e_{(\tau)}$ of τ, this becomes $x^i_{e_{(\tau)}} = \int_{e_{(\tau)}} \mathrm{x}^{ij} \mathrm{t}_{\mathrm{j}}\, d\gamma = \mathrm{x}^{ij} \mathrm{L}_{e_{(\tau)},\mathrm{j}}$, where $\mathrm{L}_{e(\tau),\mathrm{j}}$ is the edge vector related to $e_{(\tau)}$. In the same way, the stress flux for any dual face portion within τ, $\tilde{f}_{(\tau)}$, becomes $\tilde{t}_{i\tilde{f}_{(\tau)}} = \int_{\tilde{f}_{(\tau)}} \mathrm{T}_{ij}\, \mathrm{n}^{\mathrm{j}}\, d\sigma = \mathrm{T}_{ij}\, \widetilde{\mathrm{A}}^{\mathrm{j}}_{(\tau)}$, where $\widetilde{\mathrm{A}}^{\mathrm{j}}_{(\tau)}$ is the area vector related to $\tilde{f}_{(\tau)}$. By noting that for a single tetrahedron three DoFs (displacement gradients) are independent only, previous relationships can be cast in matrix form, that is: $\mathbf{S}_{(\tau)} = \mathbf{P}_{(\tau)}\, \mathbf{x}_{(\tau)}$, where $\mathbf{S}_{(\tau)}$ is the vector (written in Voigt notation) of strain tensor components, $\mathbf{P}_{(\tau)}$ is a (6 x 18) linear mapping constructed as described in (4), and $\mathbf{x}_{(\tau)}$ is the

(18 x 1) vector of displacement gradient line integrals; $\tilde{\mathbf{t}}_{(\tau)} = \widetilde{\mathbf{A}}_{(\tau)}\, \mathbf{T}_{(\tau)}$, where $\tilde{\mathbf{t}}_{(\tau)}$ is the (18 x 1) stress flux local vector, $\widetilde{\mathbf{A}}_{(\tau)}$ is the (18 x 6) area matrix, and $\mathbf{T}_{(\tau)}$ is the vector (written in Voigt notation) of stress tensor components. Similarly, local constitutive equation $T_{ij} = c^{E}_{ijkh}\, S^{kh}$ becomes $\mathbf{T}_{(\tau)} = \mathbf{C}^{\mathbf{E}}_{(\tau)}\, \mathbf{S}_{(\tau)}$ in matrix form. By combining previous relationships, the discretized local constitutive matrices $\mathbf{C}_{(\tau)} = \widetilde{\mathbf{A}}_{(\tau)} \mathbf{C}^{\mathbf{E}}_{(\tau)} \mathbf{P}_{(\tau)}$ are obtained. The global constitutive matrix $\mathbf{C}_{ij}$ is finally derived by assembling local matrices over the whole mesh.

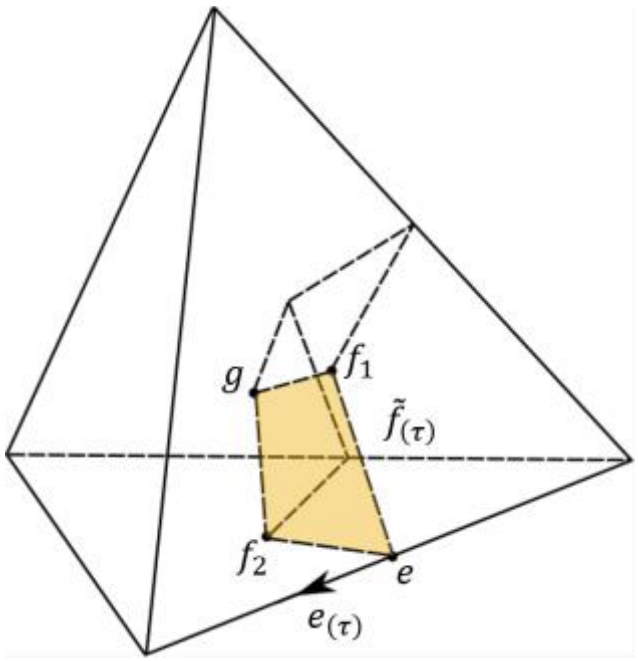

Figure 1: Primal edge $e_{(\tau)}$ within a tetrahedron τ and its corresponding dual face $\tilde{f}_{(\tau)}$ (shaded in color). The dual face vertices are the cell centroid g, the face centroids f_1, f_2, and the edge centroid e.

By inserting (7) and (8) in (5) and (6), respectively, and by using displacement and potentials as unknown variables by means of (3) and (4), a coupled linear system is obtained:

$$\begin{pmatrix} \mathbf{K_{11}} & \cdots & \mathbf{K}_{1d} & \mathbf{K}_{1\Phi} \\ \vdots & \ddots & \cdots & \vdots \\ \mathbf{K}^{\mathbf{T}}_{1d} & \cdots & \mathbf{K}_{dd} & \mathbf{K}_{d\Phi} \\ \mathbf{K}^{\mathbf{T}}_{1\Phi} & \cdots & \mathbf{K}^{\mathbf{T}}_{d\Phi} & \mathbf{K}_{\Phi\Phi} \end{pmatrix} \begin{pmatrix} \mathbf{s}^{1} \\ \vdots \\ \mathbf{s}^{d} \\ \mathbf{\Phi} \end{pmatrix} = \begin{pmatrix} -\tilde{\mathbf{f}}_{\Omega,1} + \widetilde{\mathbf{D}}_{\Omega\Gamma}\, \tilde{\mathbf{t}}_{\Gamma,1} \\ \vdots \\ -\tilde{\mathbf{f}}_{\Omega,d} + \widetilde{\mathbf{D}}_{\Omega\Gamma}\, \tilde{\mathbf{t}}_{\Gamma,d} \\ -\tilde{\mathbf{q}} + \widetilde{\mathbf{D}}_{\Omega\Gamma}\, \tilde{\mathbf{d}}_{\Gamma} \end{pmatrix}, \tag{9}$$

where $\mathbf{K}_{ij} = \mathbf{G}^{\mathrm{T}} \mathbf{C}_{ij} \mathbf{G}$ is the mechanical stiffness matrix, $\mathbf{K}_{i\Phi} = -\mathbf{G}^{\mathrm{T}} \mathbf{E}_i\, \mathbf{G}$ is the the electro-mechanical stiffness matrix, and $\mathbf{K}_{\Phi\Phi} = -\mathbf{G}^{\mathrm{T}} \boldsymbol{\varepsilon}\, \mathbf{G}$ is the the electrostatic stiffness matrix. The final coupled matrix system (9) can be written in compact form as $\mathbf{K}\,\mathbf{x} = \mathbf{f}$, where the solution vector is $\mathbf{x} = \left(\mathbf{s}^{1}, \ldots, \mathbf{s}^{\mathrm{d}}, \mathbf{\Phi}\right)^{\mathbf{T}}$. A direct solver is applied to (9) after imposing Dirichlet (displacements) and Neumann (tractions) boundary conditions.

3.1 Dynamic coupled problem

Steady state FIT formulation can be extended to dynamic coupled piezoelectric problems adding inertia forces and dumping.

The inertia force on the *i*-th dual volume $\tilde{\tau}_j$ is given by $\tilde{f}_i = \int_{\tilde{\tau}_j} \rho\, g_i(x)\, d\tau$, where g_i the *i*-th component of the acceleration and ρ the mass density. The mass matrix $\mathbf{M}_\rho = (\int_{\tilde{\tau}_j} \rho\, d\tau)$, of size $N \times N$, is diagonal in FIT. According to Rayleigh's theory, damping matrices (for mechanical problem only) are defined as a linear combination of mass and stiffness matrices, that is $\mathbf{D}_{v,ij} = \alpha\, \mathbf{M}_\rho + \beta\, \mathbf{K}_{ij}$ where α and β are damping coefficients defined experimentally.

The dynamic behaviour of the coupled piezoelectric problem in discrete form is then described by the following second order ordinary differential equation (ODE) system:

$$\mathbf{M}\,\ddot{\mathbf{x}} + \mathbf{D}\,\dot{\mathbf{x}} + \mathbf{K}\,\mathbf{x} = \mathbf{f}, \tag{10}$$

where:

$$\mathbf{M} = \begin{pmatrix} \mathbf{M}_\rho & \cdots & \mathbf{0} & \mathbf{0} \\ \vdots & \ddots & \vdots & \vdots \\ \mathbf{0} & \cdots & \mathbf{M}_\rho & \mathbf{0} \\ \mathbf{0} & \cdots & \mathbf{0} & \mathbf{0} \end{pmatrix}, \quad \mathbf{D} = \begin{pmatrix} \mathbf{D}_{v,11} & \cdots & \mathbf{D}_{v,1d} & \mathbf{0} \\ \vdots & \ddots & \vdots & \mathbf{0} \\ \mathbf{D}_{v,1d}^{\mathrm{T}} & \cdots & \mathbf{D}_{v,dd} & \mathbf{0} \\ \mathbf{0} & \mathbf{0} & \mathbf{0} & \mathbf{0} \end{pmatrix},$$

and matrix **K** is defined in (9). The ODE system (10) is solved by the Newmark-β integration scheme, that is the responses after time Δt, i.e. $\mathbf{x}_{n+1}, \dot{\mathbf{x}}_{n+1}, \ddot{\mathbf{x}}_{n+1}$, are calculated from those at the previous time step, i.e. $\mathbf{x}_n, \dot{\mathbf{x}}_n, \ddot{\mathbf{x}}_n$ and from the rhs $\mathbf{f}_{n+1}$, as

$$\begin{aligned} \boldsymbol{A}_{n+1}\, \ddot{\mathbf{x}}_{n+1} &= \mathbf{b}_{n+1}, \\ \dot{\mathbf{x}}_{n+1} &= \dot{\mathbf{x}}_n + (1-\gamma)\Delta t\, \ddot{\mathbf{x}}_n + \gamma \Delta t\, \ddot{\mathbf{x}}_{n+1}, \\ \mathbf{x}_{n+1} &= \mathbf{x}_n + \Delta t\, \dot{\mathbf{x}}_{\boldsymbol{n}} + \Delta t^2 \left[\left(\tfrac{1}{2} - \beta\right) \ddot{\mathbf{x}}_n + \beta\, \ddot{\mathbf{x}}_{n+1}\right], \end{aligned} \tag{11}$$

where:

$$\begin{aligned} \boldsymbol{A}_{n+1} &= \mathbf{M} + \gamma \Delta t\, \mathbf{D} + \beta \Delta t^2 \mathbf{K}, \\ \mathbf{b}_{n+1} &= \mathbf{f}_{n+1} - \mathbf{K}\,\mathbf{x}_n - (\mathbf{D} + \Delta t\, \mathbf{K})\, \dot{\mathbf{x}}_{\boldsymbol{n}} - \left[(1-\gamma)\Delta \mathrm{t}\, \mathbf{D} + \Delta \mathrm{t}^2 \left(\tfrac{1}{2} - \beta\right) \mathbf{K}\right] \ddot{\mathbf{x}}_n. \end{aligned}$$

The iterative time-stepping integration algorithm is proved to be unconditionally stable and convergent for a proper choice of parameters γ and β such that $4\beta \geq 2\gamma \geq 1$ [15].

3 NUMERICAL RESULTS

The static FIT model is validated by FEM results (COMSOL Multiphysics®) on a 2-D test case consisting in a multilayered PVDF bimorph beam used as an actuator, under an external voltage excitation. The dynamic FIT model is validated on a 3-D test case consisting in a

multilayered PZT bimorph cantilever harvester excited by a force impulse (e.g. which is typical for devices mounted within tires) and in electrical open circuit conditions.

3.1 PVDF bimorph beam

The piezoelectric actuator presented in [16] is considered for validating the 2-D FIT static model ($d = 2$). The plane stress assumption holds in fact with thin structures. The bimorph beam (size $20\times5\times1$ mm) consists of two piezo PVDF layers (0.5 mm thick each) with opposite polarity. A constant potential is applied to top and bottom sides of the cantilever (the bottom side is the mass electrode). Clamping BCs are applied to one end and deflection due to external voltage is then computed.

The bimorph beam model is discretized by FIT into 20,116 triangles. The assembly time for the discretized FIT model (30,982 unknowns) is 1.46 s. The system solution with direct solver requires 0.46 s on a Intel Core i7 processor (2.70 GHz).

Fig. 2 shows the tip displacement for applied voltages varying from 0 V up to 200 V. FIT results are compared with data provided in [16], showing a very good agreement. The FEM model proposed by Park is fully 3-D, being based on plate bending elements. Other data used for comparison are obtained from experimental measurements and 1-D analytical modelling.

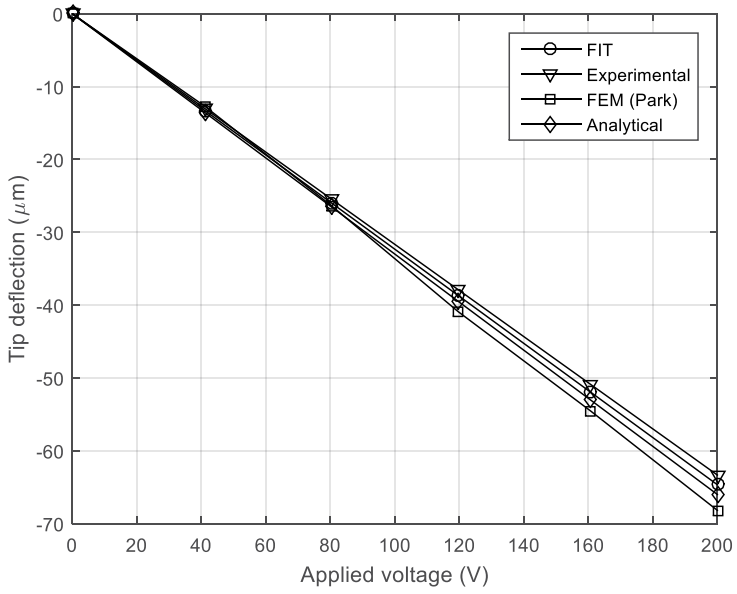

Figure 2: Tip displacement along the z-axis vs. applied voltage (experimental, FEM, and analytical data are provided in [16] for the actuator test case; FIT data are computed by a 2D FIT in-house code).

3.2 PZT bimorph cantilever

In order to validate the 3-D FIT dynamic model ($d = 3$) a commercial piezo energy harvester for feeding ultra-low power electronic devices is considered. This can be used e.g. for supplying wireless sensors used in tire pressure monitoring systems [17]. The bimorph beam, with size

25.4 x 3.81 x 0.72 mm, has a complex multi-layered structure: two inner piezo layers (0.18 mm thick each) with opposite polarization, made of lead zirconate titanate (PZT-5A), are used for charge generation, and two external layers of FR4 composite material (epoxy) are used to provide structure stiffness. The intermediate layer of Espanex® (copper conductor) is not included in the CAD geometry and is modelled simply by assuming a circuit terminal condition. The cantilever is excited by a vertical inertia force impulse, of sinusoidal waveform, to simulate the typical excitation experienced by the harvester mounted inside a rotating tire [18]:

$$g_z(x,t) = -\rho\, P\, \mathrm{rect}\left(\frac{t}{\delta}\right) \sin\left(\pi \frac{t}{\delta}\right), \tag{12}$$

where ρ is the mass density, P the pulse amplitude, rect is the unit rectangular function, and δ is the pulse width. Constant (unknown) potentials are imposed at top and bottom sides of the piezo structure. Clamping boundary conditions are applied to one end of the cantilever.

The displacement and voltage system responses are simulated by 3-D FEM and the 3-D FIT dynamic model illustrated in Section 2. FIT formulation is coded in Matlab® in a vectorized language style to speed-up computations. The model geometry is meshed into 160,948 tetrahedrons, 203,882 edges, and 32,369 nodes. First order elements are used for mechanics and electrostatics coupled physics with FEM, whereas affined basis functions are used with FIT. Note that a transient 3-D FEM model with second order elements, for the test case considered, is computationally unfeasible due to the huge number of DoFs. The assembly time for the discretized FIT model (106,639 unknowns) is 30.02 s. The system solution at each time step requires 7.29 s on the same machine as above. To finely resolve the electromechanical transient, a sufficiently small time step $\Delta t = 0.005\ \delta$ is set for both FEM and FIT, with $t_{max} = 10\ \delta$ analysis time. Different integration schemes are used: BDF (5th order backward differentiation, to get an accurate integration) for COMSOL® and Newmark-β for FIT. The simulation time of transient analysis is 4 h 23 min for the COMSOL® solver and 4 h 28 min for the FIT code. Electromechanical constitutive tensors for FR4 and PZT-5A are taken from the COMSOL® material library. Other relevant parameters for simulations are P = –9.81 m/s^2, δ = 1.5 ms for the force impulse, and $\alpha = 0$ s^{-1}, $\beta = 4 \cdot 10^{-6}$ s for damping.

In order to compare FEM and FIT analyses the open circuit voltage and the displacement at the center of the cantilever are computed. Fig. 3 and 4 show that FIT time responses agree very well with FEM, even though different time integrators have been used. Maximum discrepancy values between FEM-FIT distributions are 0.21 % for voltage and 0.20 % for displacement.

Finally, spatial solutions at the last time step are compared to estimate overall accuracy of the FIT model. A horizontal line of coordinates x = [0, 25.4] mm, y = 1.905 mm, z = 0.36 mm, placed along the cantilever horizontal axis, is considered (Fig. 5). Fig. 6 and 7 show that profiles of the z–axis displacement component, computed along the beam axis for the most significant time steps $t = t_{max}/2$ and $t = t_{max}$, agree very well with FEM. Maximum discrepancy values between FEM-FIT distributions are 0.05 % ($t = t_{max}/2$) and 0.02 % ($t = t_{max}$), respectively.

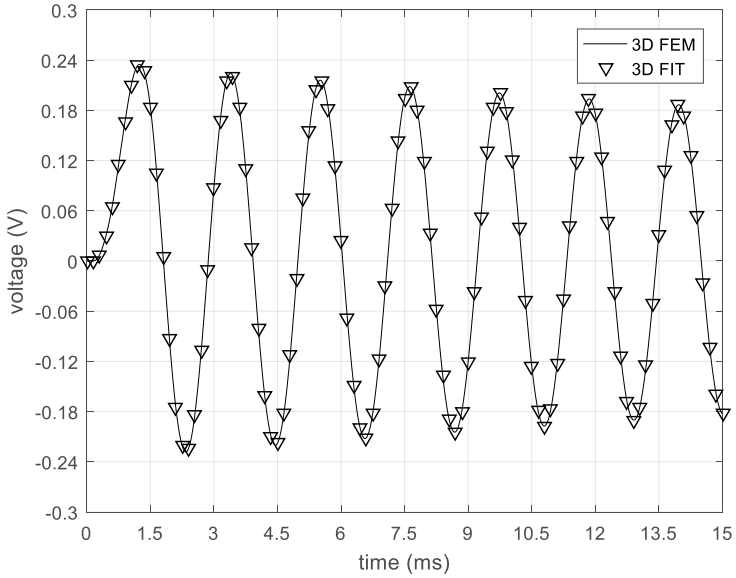

Figure 3: Open circuit voltage response for 1g acceleration pulse (3-D FEM: straight line, 3-D FIT: markers).

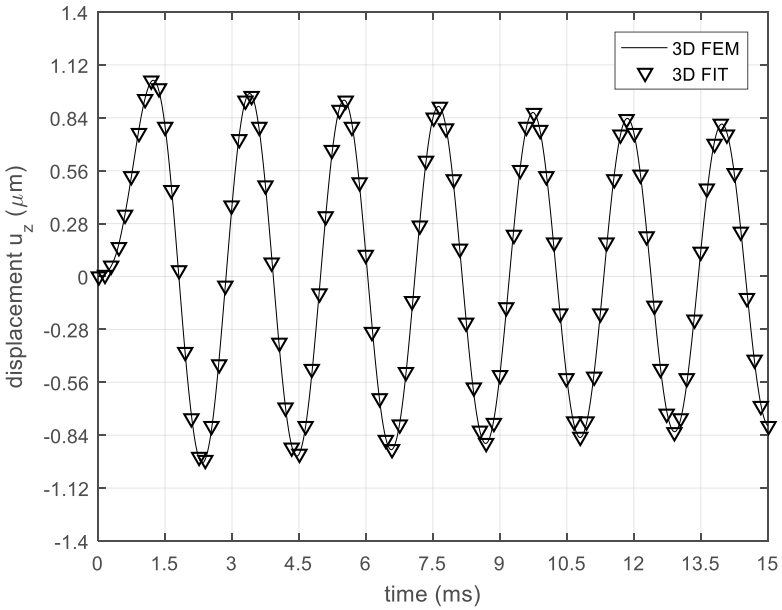

Figure 4: z–axis displacement component at the center of the cantilever for 1g acceleration pulse (3-D FEM: straight line, 3-D FIT: markers).

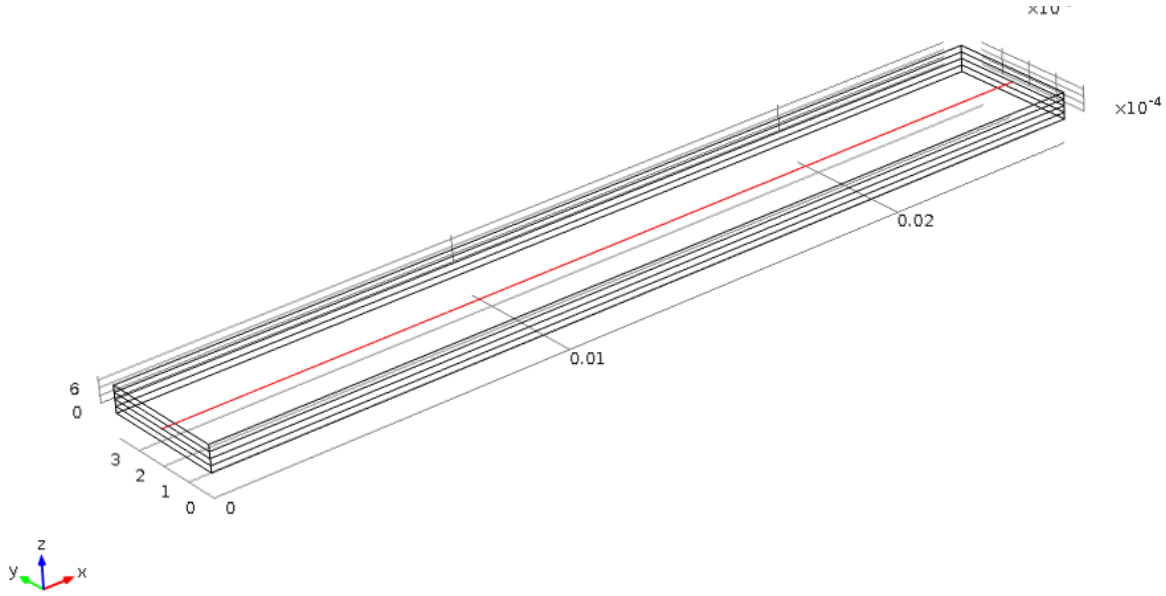

Figure 5: Horizontal line along the beam axis (x = [0, 25.4] mm, y = 1.905 mm, z = 0.36 mm; red color).

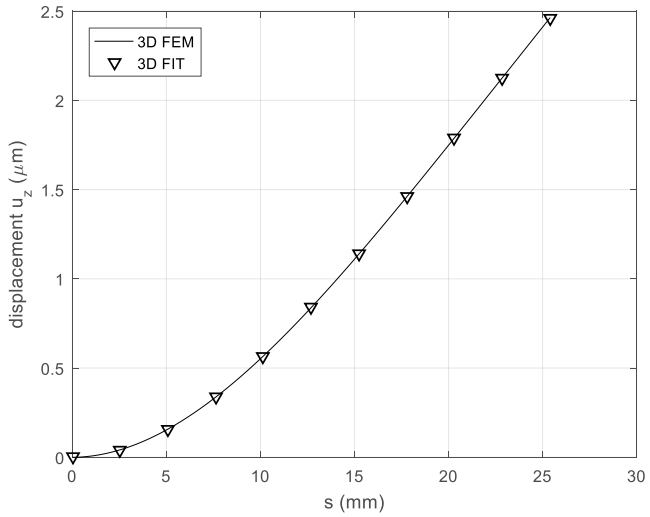

Figure 6: z–axis displacement component along the beam axis at the time step $t = t_{max}/2$ (evaluated at points on x = [0, 25.4] mm, y = 1.905 mm, z = 0.36 mm; 3-D FEM: straight line, 3-D FIT: markers).

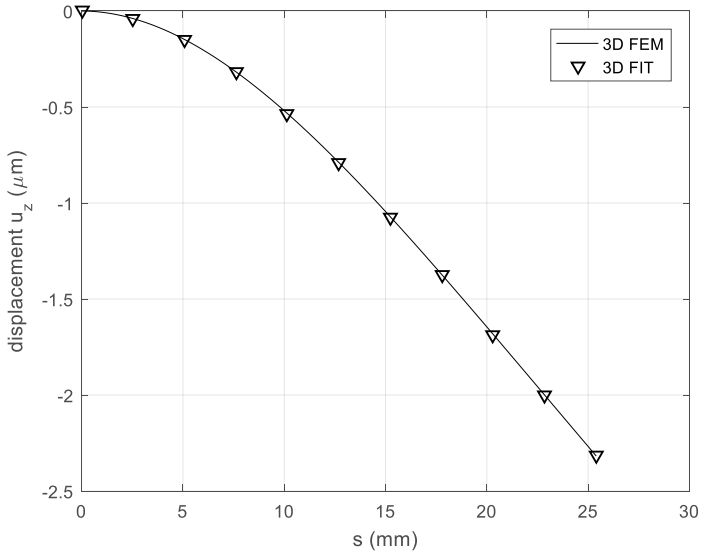

Figure 7: z–axis displacement component along the beam axis at the last time step $t = t_{max}$ (evaluated at points on x = [0, 25.4] mm, y = 1.905 mm, z = 0.36 mm; 3-D FEM: straight line, 3-D FIT: markers).

11 ACKNOWLEDGMENT

This work was supported by the Università di Padova under the Grant CPDA142798 (project PRAT14 “Piezoelectric Micro-Electro-Mechanical Power Supply for Automotive Wireless Sensors”).

12 CONCLUSIONS

This work demonstrates that FIT, for tetrahedral meshes, also extends to piezoelectric problems by assuming a local affine displacement vector field. The building strategy for local constitutive matrices is similar to that one used for elastic problems. In such a way, topological and constitutive relationships are split and the construction of the final coupled system becomes simpler and can be solved in a matrix-oriented numerical environment such as Matlab®. Test cases show that FIT code is accurate and reliable even with 3-D numerical models of commercial cantilevers, exhibiting a complex multilayered and multi-material structure.

REFERENCES

[1] Rincón-Mora, G. A. and Yang, S. Tiny Piezoelectric Harvesters: Principles, Constraints, and Power Conversion. *IEEE Trans. on Circuits and Systems I: Regular Papers* (2016) **63**: 639–649.

[2] Priya, S., and Inman, D.J. *Energy Harvesting Technologies*. Springer-Verlag (2009).

[3] Kázmierski, T.J., and Beeby, S. *Energy Harvesting Systems: Principles, Modelling, and Applications*. Springer-Verlag (2011).

[4] De Marqui, C., Erturk, A, and Inman, D.J. An electromechanical finite element model for piezoelectric energy harvester plates. *Journal of Sound and Vibration* (2009) **327**: 9-25.

[5] Lam, K.Y., Peng, X.Q., Liu, G.R., and Reddy, J.N. Finite element model for composite laminates. *Smart Materials & Structures* (1997) **6**: 583–591.

[6] Alotto, P., Freschi, F., Repetto, M., and Rosso, C. *The Cell Method for Electrical Engineering and Multiphysics problems. An Introduction*. Lecture Notes in Electrical Engineering 230, Springer (2013).

[7] Alotto, P., Freschi, F., and Repetto, M. Multiphysics problems via the cell method: The role of Tonti diagrams. *IEEE Trans. Magn.* (2010) **46**: 2959–2962.

[8] Alotto, P., Bullo, M., Guarnieri, M., and Moro, F. A Coupled Thermo–Electromagnetic Formulation Based on the Cell Method. *IEEE Trans. Magn*. (2008) **44**: 702–705.

[9] Alotto, P., Guarnieri, M., Moro, F. A mortar cell method for electro-thermal contact problems. *IEEE Trans. Magn.* (2013), **49**: 795–798.

[10] Moro, F., and Codecasa, L. Indirect Coupling of the Cell Method and BEM for Solving 3–D Unbounded Magnetostatic Problems. *IEEE Trans. Magn.* (2016) **52**: Art. ID 7200604.

[11] Tonti, E., and Zarantonello, F. Algebraic formulation of elastostatics: The Cell Method. *Comput. Modeling Eng. Sci.* (2009) **39**: 201–236.

[12] Bossavit, A. Discrete magneto-elasticity: A geometrical approach. *IEEE Trans. Magn.* (2010) **46**: 3485–3491.

[13] Moro, F., Alotto, P., Freschi, F., and Guarnieri, M. A Cell Method Formulation of 3-D Electrothermomechanical Contact Problems With Mortar Discretization. *IEEE Trans. Magn.* (2012) **48**: 503–506.

[14] Codecasa, L. Refoundation of the Cell Method Using Augmented Dual Grids. *IEEE Trans. Magn*. (2014) **50**: pp. 497–500.

[15] Kagawa, Y., et al. Finite Element Simulation of Dynamic Responses of Piezoelectric Actuators. *Journal of Sound and Vibration* (1996) **191**: 519-538.

[16] Hwang, W.S., and Park, H.C. Finite Element Modelling of Piezoelectric Sensors and Actuators. *AIAA Journal* (1993) **31**: 930–937.

[17] Mak, K.H., McWilliam, S., and Popov, A. Piezoelectric energy harvesting for tire pressure measurement applications. *Proc. Mech. E Part D: J Automobile Engineering* (2013) **227**: 842–852.

[18] Doria, A., Moro, F., Desideri, D., Maschio, A., and Zhang, Z. An impulsive method for the analysis of piezoelectric energy harvesters for intelligent tires. *Proc. ASME Int. Design Engineering Technical Conference IDETC 2016, Charlotte, USA (August 21-24, 2016).*